HEAT TRANSFER ASIAN RESEARCH

EDITOR-IN-CHIEF: PROFESSOR William. M. Worek

Frank H. Dotterweich College of Engineering, Texas A&M University-Kingsville, Kingsville, Texas, USA.

PUBLISHER- WILEY USA

ONLINE ISSN: 1523-1496

ACCEPTED JUNE 28th 2018

LIE SYMMETRY ANALYSIS AND NUMERICAL SOLUTIONS FOR THERMO-SOLUTAL CHEMICALLY-REACTING RADIATIVE MICROPOLAR FLOW FROM AN INCLINED POROUS SURFACE

MD. Shamshuddin[1*]
[1*]*Department of Mathematics, Vaagdevi College of Engineering, Warangal, Telangana,* ***India.***
Email: shammaths@gmail.com
Contact No: +91-9866826099

S.R. Mishra[2]
[2]*Department of Mathematics, Siksha 'O'Anusandhan University, Khandagiri, Bhubaneswar, Odisha,* ***India.***
Email: satyaranjan_mshr@yahoo.co.in

O. Anwar Bég[3]
[3]*Aeronautical and Mechanical Engineering, University of Salford, Manchester, England,* ***UK.***
Email: gortoab@gmail.com, O.A. Beg@salford.ac.uk

Ali Kadir[4]
[4]*Materials, Corrosion and Structures, Aeronautical and Mechanical Engineering, School of Computing, Science and Engineering, Newton Building, Salford, M54WT, England,* ***UK.***
Email: a.Kadir@salford.ac.uk

*******Corresponding author: shammaths@gmail.com, mdshamshuddin@vaagdevieng.ac.in*

ABSTRACT

Steady, laminar, incompressible thermo-solutal natural convection flow of micropolar fluid from an inclined perforated surface with convective boundary conditions is studied. Thermal radiative flux and chemical reaction effects are included to represent phenomena encountered in high-temperature materials synthesis operations. Rosseland's diffusion approximation is used to describe the radiative heat flux in the energy equation. A Lie scaling group transformation is implemented to derive a *self-similar* form of the partial differential conservation equations. The resulting coupled nonlinear boundary value problem is solved with Runge-Kutta fourth order numerical quadrature (shooting technique). Validation of solutions with an optimized Adomian decomposition method algorithm is included. Verification of the accuracy of shooting is also conducted as a particular case of *non-reactive micropolar flow from a vertical permeable surface*. The evolution of velocity, angular velocity (micro-rotation component), temperature and concentration are examined for a variety of parameters including coupling number, plate inclination angle, suction/injection parameter, radiation-conduction parameter, Biot number and reaction parameter. Numerical results for steady state skin friction coefficient, couple stress coefficient, Nusselt number and Sherwood number are tabulated and discussed. Interesting features of the hydrodynamic, heat and mass transfer characteristics are examined.

KEYWORDS: *Thermal radiation, chemical reaction, micropolar fluid, Lie symmetry analysis, shooting method, Adomian decomposition.*

1. INTRODUCTION

Non-Newtonian materials processing [1] is a rich and vibrant area of modern fluid dynamics research providing a multi-disciplinary platform for theoretical, computational and laboratory-based investigations. Many different polymeric materials exist which exhibit a considerable range of shear-stress strain relationships that do not obey the classical Newtonian model. In many processes a polymer flows along a continuously moving belt which may be horizontal or *inclined*. When heat and mass transfer are also present, buoyancy effects become significant. Thermal treatment and species doping are common strategies employed in engineering materials for modern applications. *Inclination* may be effectively used to scale the contribution of thermal and solutal buoyancy forces. These can strongly influence the diffusion of heat and species in materials. The fundamental approach for simulating such flows is *boundary-layer theory*. Examples of applications of inclined plane non-Newtonian flows include rheometry [2], powder processing [3], thin film coating systems [4], environmental gravity-driven debris flows (landslides,

avalanches, mudslides, hazards) [5, 6]. When heat and mass transfer are also present in inclined plate flows with free convection and multi-physical effects (e.g. combustion, magnetic fields, electrical fields etc.), the resulting scenarios feature in many diverse technologies including plate fin heat sinks [7], external transport from titled solar collectors [8], geothermal energy heat pumps [9], flame dynamics [10], laser materials processing [11], hybrid desalination configurations [12] and supercritical flows in geothermosiphons [13]. Classical experimental studies of thermal convection flows from inclined plate geometries were presented by Shaukatullah and Gebhart [14] and Hasan *et al.* [15]. More recently Cianfrinia *et al.* [16] investigated thermal boundary flows from inclined plates. These studies however were confined to Newtonian fluids. Many different models have been implemented for non-Newtonian transport phenomena from inclined surfaces. These include Ostwald-DeWaele pseudo plastic models [17], dilatant power-law fluids [18], variable-viscosity (Reynolds) fluid [19], Jeffrey's viscoelastic fluids [20], third grade differential fluids [21], viscoplastic fluids [22], modified power-law fluids [23] and couple stress fluids [25].

The above studies have generally neglected *micro-structural* features of the fluid. Even the most sophisticated viscoelastic models cannot provide a framework for this since they merely modify the shear stress tensor to include supplementary derivatives aimed at simulating (to varying degrees of accuracy) stress relaxation, retardation, shear thickening/thinning and other simple effects. Many polymeric and industrial fluids (propellants, gels, coolants etc) exist which possess a complex micro-structure that effectively contributes strongly to their performance characteristics. Motivated by constructing a comprehensive and rigorous continuum mechanics framework for addressing these fluids, Eringen [26] introduced *micro-morphic fluid mechanics* in the 1960s. He further derived the micropolar fluid model [27] as a special case of micro-morphic fluids with non-deformable micro-elements. A tremendous benefit of the micropolar model is that it reduces the original eighteen balance equations to a maximum of six momenta balance equations (three for linear and three for angular). Further it allows the extraction of the Navier-Stokes classical viscous model as a very special case when micro-morphic effects are negated. The elegance of Eringen's micropolar model has led to its adoption in a stunning range of applications. Building on fundamental solutions laid out in [25], and extended by Ariman and Cakmak [26], micropolar fluid mechanics has been applied to adhesive systems [27], hemodynamics [28], subsonic gas dynamics [29], bio-tribology [30], drilling muds for petroleum reservoirs [31], coating flows of aerospace propulsion ducts [32], drainage systems [33], magnetic materials processing [34], digestive propulsion [35] and geothermal systems [36]. A superb summary of the thermodynamics and hydrodynamics of micropolar fluids is provided in Eringen [37]. A number of inclined plate micropolar flow

models have also been developed, largely motivated by petro-chemical and materials fabrication applications. Probably the first study of micropolar flow from an inclined surface was conducted by Wilson [38], who examined the hydrodynamic stability of thin film gravity-driven micropolar flow from an inclined plate using Yih's expansion method, noting the significant influence of vortex viscosity on the delay of instability. Thermal convection in micropolar flow from an inclined plate was addressed by Rahman *et al.* [39] with Nachtsheim–Swigert iteration procedure. Das *et al.* [40] employed symbolic software Mathematica 7 to analyze reactive magnetic thermo solutal micropolar slip flow from an inclined plate with viscosity and thermal conductivity variation. Srinivasacharya and Bindu [41] used a spectral quasilinearization method to compute entropy generation under constant pressure gradient, noting a significant enhancement in Bejan number increases with greater plate inclination and also Brinkman number and a decrease with micropolar coupling number. Bég *et al.* [43] employed a network simulation code to analyze the magnetohydrodynamic thin film flow of a micropolar fluid from an inclined surface.

In many manufacturing processes, *high temperature* conditions are imposed. These often invoke substantial contributions from thermal radiation heat transfer which may be employed to enhance anti-degradation characteristics of materials [43, 44]. Non-Newtonian radiative flow has been studied therefore by Cortell [45] although he employed a group of viscoelastic models (second-grade and Walters' liquid B models). More realistic simulations of actual high-temperature materials processing therefore require simultaneous consideration of *thermal conduction, convection and radiation*. When the fluids are electro-conductive, magnetohydrodynamics must also be considered. Usually the most challenging aspect is the robust analysis of radiative heat flux. Many sophisticated models exist for a range of materials which capture complex radiative properties including transmission, reflection, absorption, gray, non-gray, opaqueness, variable optical thickness, specular and spectral aspects. However, to formulate boundary value problems which are solvable with most numerical methods it is necessary to simplify the integro-differential radiative transfer equation (RTE) to a flux model. Examples include Hamaker's six flux model and the Rosseland diffusion approximation. These approaches transform the RTE into a system of algebraic equations which can be accommodated easily with iterative procedures, as elaborated by Viskanta [46].

In the present work we develop a mathematical model for *radiative micropolar thermo-solutal transport from a tilted two-dimensional permeable plate under steady-state conditions*. The micropolar fluid contains a chemically-reactive species [35] and suction/injection effects are present at the plate. A convective boundary condition is also enforced at the plate. Lie group algebra is employed to extract a self-similar boundary value problem from the primitive partial

differential conservation equations. Shooting quadrature computational solutions are developed to elucidate the influence of Biot number, chemical reaction parameter, Eringen micropolar coupling number, plate inclination angle, suction/injection parameter, radiation-conduction parameter, Biot number on the key characteristics. Validation is included based on earlier studied and also with an optimized Adomian decomposition method (ADM) [47]. Extensive interpretation of computations is provided.

2. REACTIVE RADIATIVE MICROPOLAR THERMO-SOLUTAL MODEL

2.1 Problem formulation:

We examine the two-dimensional, steady-state, incompressible, natural convective heat and mass transfer in the flow of an incompressible micropolar fluid from an infinite inclined moving porous plate orientated at an acute angle $\left(0^o \le \alpha \le 90^o\right)$ to the vertical and suspended in a homogenous, isotropic, porous medium. The flow model with associated coordinate system is depicted in **Fig. 1**.

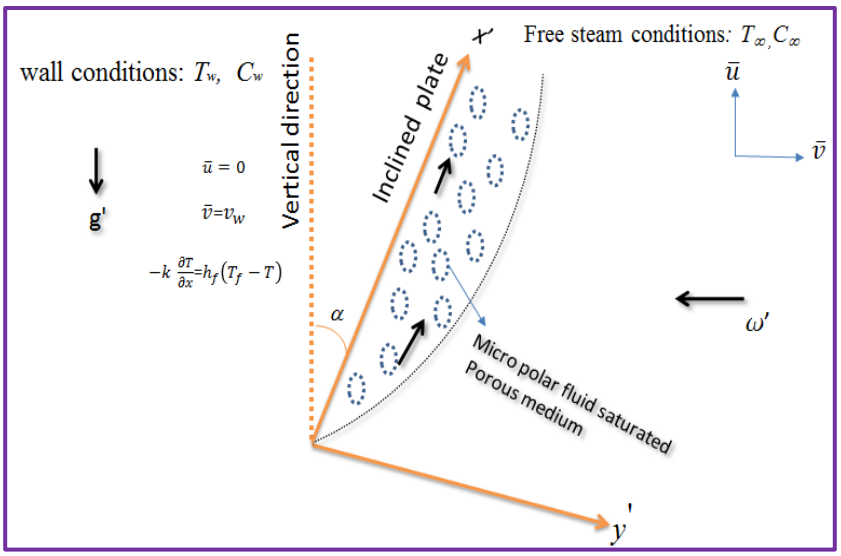

Figure 1: Flow Geometry of the problem

Inclination angles with values of $0^o, 90^o$ and $0^o \le \alpha \le 90^o$ respectively signify the vertical, horizontal and inclined plate scenarios. The flow is assumed to be in the x-direction, and the y -axis is normal to it. It is assumed the free stream temperature and concentration are T_∞ and C_∞ respectively. The plate is either heated or cooled from the left by convection from micropolar fluid of temperature T_f with $T_f > T_\infty$ corresponds to a heated surface (assisting flow) and $T_f < T_\infty$ corresponds to a cooled surface (opposing flow). The suction/injection velocity invoked by the plate

porosity is assumed as v_w.Viscous dissipation and thermal dispersion and stratification effects are ignored. Thermal conduction follows the Fourier model. Further, the micropolar fluid contains a species which is reactive and obeys a first order homogenous chemical reaction. We assumed that the size of holes in the porous plate plays an important role to simplify the formulation of the boundary conditions. By taking the aforesaid assumptions into consideration the governing boundary layer equations with corresponding boundary conditions [48] for steady convective flow are as follows:

$$\frac{\partial u'}{\partial x'}+\frac{\partial v'}{\partial y'}=0 \tag{1}$$

$$u\frac{\partial u'}{\partial x'}+v'\frac{\partial u'}{\partial y'}=\left(\frac{\mu+k}{\rho}\right)\frac{\partial^2 u'}{\partial y'^2}+g\beta_T\left(T-T_\infty\right)\cos\alpha+g\beta_C\left(C-C_\infty\right)\cos\alpha+\frac{k}{\rho}\frac{\partial N'}{\partial y'} \tag{2}$$

$$u'\frac{\partial N'}{\partial x'}+v'\frac{\partial N'}{\partial y'}=\frac{\gamma}{\rho\, j'}\frac{\partial^2 N'}{\partial y'^2}-\frac{k}{\rho\, j'}\left(\frac{\partial u'}{\partial y'}+2N'\right) \tag{3}$$

$$u'\frac{\partial T}{\partial x'}+v'\frac{\partial T}{\partial y'}=\frac{\kappa}{\rho C_p}\frac{\partial^2 T}{\partial y'^2}-\frac{1}{\rho C_p}\frac{\partial q_r}{\partial y'} \tag{4}$$

$$u'\frac{\partial C}{\partial x'}+v'\frac{\partial C}{\partial y'}=D\frac{\partial^2 C}{\partial y'^2}-K_r'\left(x'\right)\left(C'-C_\infty\right) \tag{5}$$

$$\left.\begin{array}{l} at\ y'=0\ \left\{\ u'=0,\ v=v_w,\ N'=-n\dfrac{\partial u'}{\partial y'},\ \dfrac{\partial T}{\partial y'}=-\dfrac{h_f}{k}\left(T_f-T\right),\ C=C_w\right. \\ as\ y'\to\infty\ \left\{\ u'\to 0, N'\to 0,\ T\to T_\infty,\ C\to C_\infty\right. \end{array}\right\} \tag{6}$$

Here u' and v' are velocity components along x' and y' axis respectively, N' is the micro-rotation component (i.e. gyratory motion of micro-elements is in the x' - y' plane), ρ is the density of micropolar fluid, μ is the dynamic viscosity, k is the Eringen vortex viscosity, g is the acceleration due to gravity, β_T and β_C are coefficient of thermal expansion and concentration expansion, γ is a material property (gyroscopic viscosity) of the micropolar fluid, j' is the micro inertia per unit mass , and κ is thermal conductivity of the micropolar fluid. At constant pressure p, C_p is the specific heat, q_r is the radiative heat flux, D is the molecular diffusivity of the reactive species. The surface parameter n assumes values between 0 and 1 that quantifies the relationship between the micro-gyration vector to the shear stress. When $n=0$, this corresponds to the case where the micro-element (particle) density is sufficiently large so that microelements close to the wall are not able to rotate [49]. When $n=0.5$ this indicates weak concentration of micro-elements and the disappearance of the anti-symmetric part of stress tensor, as elaborated by Ahmadi [50].

When $n=1.0$ represents turbulent boundary layer flows as described by Peddieson [51] and Stokes [52]. However, when $n=0.5$ or $n=1.0$ this case tends to accelerate the flow [51, 52]. It is also important to note that in the micro-polar theory vectors are considered to be *rigid directors* as the micro-elements are *non-deformable*.

Introducing the following no-dimensional variables

$$\left.\begin{aligned} x=\frac{x'}{L},\ \ y=\frac{y'}{L}Gr^{1/4},\ \ u=\frac{L}{\nu\sqrt{Gr}}u',\ \ v=\frac{L}{\nu\, Gr^{1/4}}v',\ N=\frac{L^2}{\nu\, Gr^{3/4}}N' \\ \theta=\frac{T-T_\infty}{T_f-T_\infty},\ \varphi=\frac{C-C_\infty}{C_w-C_\infty},Gr=\frac{g'\beta_T\left(T_f-T_\infty\right)L^3}{\nu^2} \end{aligned}\right\} \tag{7}$$

Following the Rosseland radiative diffusion approximation [53],

$$q_r=\frac{-4\bar{\sigma}}{3\bar{k}}\frac{\partial T^4}{\partial y'} \tag{8}$$

Here $\bar{\sigma}$ is the Stefan-Boltzmann constant and $\bar{k}$ is the mean absorption coefficient. Using Taylor's series expansion about T', the expansion of T'^4 can be written as follows, neglecting higher order terms:

$$T'^4\cong 4T_\infty'^3T-3T_\infty'^4 \tag{9}$$

Therefore, equation (3), after differentiating w.r.t y' equation (8) using (9), emerges as:

$$u'\frac{\partial T}{\partial x'}+v'\frac{\partial T}{\partial y'}=\frac{\kappa}{\rho C_p}\left(1+\frac{16\bar{\sigma}}{3\bar{k}\,\kappa}T_\infty^3\right)\frac{\partial^2 T}{\partial y'^2} \tag{10}$$

Furthermore, by introducing a dimensional stream function ψ defined by $u=\frac{\partial\psi}{\partial y}$, $v=-\frac{\partial\psi}{\partial x}$ into equations (2)- (6), we have

$$\frac{\partial\psi}{\partial y}\frac{\partial^2\psi}{\partial x\,\partial y}-\frac{\partial\psi}{\partial x}\frac{\partial^2\psi}{\partial y^2}=\left(\frac{1}{1-K}\right)\frac{\partial^3\psi}{\partial y^3}-\left(\frac{K}{1-K}\right)\frac{\partial N}{\partial y}+\frac{g'\beta_T\left(T_f-T_\infty\right)L^3}{\nu^2 Gr}\theta\cos\alpha+\frac{g'\beta_C\left(C_w-C_\infty\right)L^3}{\nu^2 Gr}\varphi\cos\alpha \tag{11}$$

$$\frac{\partial\psi}{\partial y}\frac{\partial N}{\partial x}-\frac{\partial\psi}{\partial x}\frac{\partial N}{\partial y}=\left(\frac{2-K}{2-2K}\right)\frac{\partial^2 N}{\partial y^2}-\left(\frac{K}{1-K}\right)\left(2N+\frac{\partial^2\psi}{\partial y^2}\right) \tag{12}$$

$$\frac{\partial\psi}{\partial y}\frac{\partial\theta}{\partial x}-\frac{\partial\psi}{\partial x}\frac{\partial\theta}{\partial y}=\frac{1}{Pr}(1+R)\frac{\partial^2\theta}{\partial y^2} \tag{13}$$

$$\frac{\partial\psi}{\partial y}\frac{\partial\varphi}{\partial x}-\frac{\partial\psi}{\partial x}\frac{\partial\varphi}{\partial y}=\frac{1}{Sc}\frac{\partial^2\varphi}{\partial y^2}-Kr\varphi \tag{14}$$

$$\left.\begin{array}{l} at\ \ y=0 \quad \left\{\dfrac{\partial \psi}{\partial y}=0, \dfrac{\partial \psi}{\partial x}=f_w, N=-n\dfrac{\partial^2 \psi}{\partial y^2}, \ \ \dfrac{\partial \theta}{\partial y}=-Bi(1-\theta),\ \varphi=1\right. \\ as\ \ y\to\infty \quad \left\{\dfrac{\partial \psi}{\partial y}\to 0,, N\to 0, \ \ \theta\to 0,\ \varphi\to 0\right. \end{array}\right\} \tag{15}$$

Here ν is the kinematic viscosity, $Pr=\nu\rho Cp/\kappa=\mu Cp/\kappa$, is the Prandtl number, $Sc=\nu/D$ is the Schmidt number, $N=k/(\mu+k)$ is the Eringen micropolar coupling number $(0\le N<1)$, $j=L^2/\sqrt{Gr}$ is micro inertia density (where *Gr* is the thermal Grashof number) and $R=16\bar{\sigma}T_\infty^3/3\bar{k}\kappa$ is the radiation-conduction parameter, also variously known as the Stark number and Boltzmann number.

2.2 Transformation of primitive equations by Lie group algebraic analysis:

The solution of the system of non-similar partial differential equations (11)- (14) subject to the boundary conditions (15) is analytically not possible. Numerical methods are required. However, even with powerful algorithms, the equations remain challenging and expensive also. Therefore, it is necessary to transform these into self-similar ODEs using Lie group transformations. This effectively reduces the number of independent variables of the governing partial differential equations. Lie algebra is a powerful analytical approach based on continuous symmetry of mathematical structures and objects which has found many uses in modern theoretical physics and applied mathematics. This theory provides a new methodology for analyzing the continuous symmetries of governing equations of many fluid dynamic systems including non-Newtonian transport phenomena. Reviews for the fundamental theory and applications of Lie group analysis to differential equations may be found in the text books by Olver [54], Bluman and Kumei [55], Cantwell [56]. Recently many researchers have been adopting Lie group transformations technique in various fluid flows, including Reddy and Chamkha [57] and Si *et al.* [58] for thermophysical boundary layer flows on inclined and horizontal plates, Latif *et al*. [59] for micropolar slip bio convection flows and Uddin *et al.* [60] for magnetized slip heat transfer. Defining:

$$\Gamma:\begin{cases} x=e^{-\varepsilon c_1}x^*, y=e^{-\varepsilon c_2}y^*, \ \ \psi=e^{-\varepsilon c_3}\psi^*, \ \ N=e^{-\varepsilon c_4}N^*, \ \theta=e^{-\varepsilon c_5}\theta^*, \\ \varphi=e^{-\varepsilon c_6}\varphi^*, \beta_T=e^{-\varepsilon c_7}\beta_T^*, \ \beta_C=e^{-\varepsilon c_8}\beta_C^*, \ \ j=e^{-\varepsilon c_9}j^*, \ \gamma=e^{-\varepsilon c_{10}}\gamma^* \end{cases} \tag{16}$$

Here $\varepsilon\neq 0$ is the parameter of the Lie group Γ and $c_i's\ (i=1,2,.....10)$ are arbitrary real numbers which are not all zeros. We seek the values of $c_i's\ (i=1,2,.....10)$ such that equations (11) – (14) remain *invariant* under these

transformations as in [48]. These are in fact *absolute invariants* under this group of transformation and are those functions having the same form before and after the transformations. They are connected as follows:

$$\left.\begin{array}{l} c_1 = c_3 = c_4 = c_7 = c_8 = c_9 = c_{10} \\ and \\ c_2 = c_5 = c_6 = 0 \end{array}\right\} \tag{17}$$

The characteristic equations are therefore:

$$\frac{dx}{c_1 x} = \frac{dy}{0} = \frac{dx}{c_1 x} = \frac{d\psi}{c_1 \psi} = \frac{dN}{c_1 N} = \frac{d\theta}{0} = \frac{d\varphi}{0} = \frac{d\beta_T}{c_1 \beta_T} = \frac{d\beta_c}{c_1 \beta_c} = \frac{d\ j}{c_1\ j} = \frac{d\ \gamma}{c_1\ \gamma} \tag{18}$$

Solving equations (18) we get:

$$\left.\begin{array}{l} \eta = y,\ \ \psi = x\ f(\eta), N = x\ h(\eta),\ \beta_T = \beta_{T_0}\ x,\ \beta_c = \beta_{c_0}\ x, \\ \theta = \theta(\eta), \varphi = \varphi(\eta),\ \ j = j_0\ x,\ \gamma = \gamma_0\ x \end{array}\right\} \tag{19}$$

Here β_{T_0}, β_{c_0} are constant thermal and mass coefficients of expansion, j_0, γ_0 are microinertia density and micropolar spin gradient viscosity, respectively.

2.3 Similarity ordinary differential equations:

Substituting Eqn. (19) into Eqns. (11)- (14), yields the following transformed, dimensionless, 9th order nonlinear system of ordinary differential equations:

$$\left(\frac{1}{1-N}\right) f''' + f\ f'' - (f')^2 + \left(\frac{N}{1-N}\right) h' + (\theta + B\varphi)\cos\alpha = 0 \tag{20}$$

$$\left(\frac{2-N}{2-2N}\right)\ h'' + f\ h' - f'\ h - \left(\frac{N}{1-N}\right)(2h + f'') = 0 \tag{21}$$

$$(1+R)\theta'' + Pr\ f\ \theta' = 0 \tag{22}$$

$$\varphi'' + Sc\ f\ \varphi' - Sc\ Kr\ \varphi = 0 \tag{23}$$

The boundary conditions (15) are converted to:

$$\left.\begin{array}{l} at\ \ \eta = 0 \quad \{\ \ f(0) = f_w, f'(0) = 0, h(0) = -n\ f''(0),\ \ \theta'(0) = -Bi(1-\theta(0)),\ \varphi(0) = 1 \\ as\ \ \eta \to \infty\ \{\ \ f'(\infty) \to 0, , h(\infty) \to 0,\ \ \theta(\infty) \to 0,\ \varphi(\infty) \to 0 \end{array}\right\} \tag{24}$$

Here primes denote the differentiation w.r.t η, $B = \beta_{c_0}(C_w - C_\infty) / \beta_{T_0}(T_f - T_\infty)$ is the buoyancy ratio parameter (species i.e. solutal buoyancy force to thermal buoyancy force ratio), $Bi = h_f\ L / kGr^{1/4}$ is the Biot number,

$f_w = -\left(L/\nu\, Gr^{1/4}\right)v_w$ is the wall lateral mass flux (suction/injection) parameter in which for suction $f_w > 0$, for injection (blowing) $f_w < 0$ and for a solid (impermeable) plate surface, $f_w = 0$ .Note that all parameters are free from χ which confirms the true similarity solution of Eqns. (20)- (23) subjected to boundary conditions (24).

2.4 Quantities of engineering interest:

Gradients of the key variables at the plate surface are important for engineering design considerations, in particular in materials processing. Here $\tau_w = \left((\mu + k)\frac{\partial \bar{u}}{\partial \bar{y}} + k\bar{N} \right)_{\bar{y}=0}$ is dimensional wall shear stress, $m_w = \gamma\left(\partial \bar{N}/\partial \bar{y}\right)_{\bar{y}=0}$ is dimensional wall couple stress, $q_w = -\kappa\left(\partial T/\partial \bar{y}\right)_{\bar{y}=0}$ is wall heat transfer coefficient and $q_m = -D(\partial C/\partial \bar{y})_{\bar{y}=0}$ is species (mass) transfer coefficient. The reduced non-dimensional skin friction $C_f = 2\tau_w/\rho \bar{u}_*^2$, takes the form:

$$C_f = \frac{2}{(Gr_{x'})^{1/4}}\left(\frac{1-nN}{1-N}\right) f''(0), \tag{25}$$

The non-dimensional wall couple stress coefficient i.e. wall micro-rotation gradient $C_w = c_w/\rho \bar{u}_*^2$ may be defined as:

$$C_w = \frac{1}{\sqrt{Gr_{x'}}}\left(\frac{2-N}{2-2N}\right) h'(0), \tag{26}$$

The non-dimensional local Nusselt number $Nu = q_w/k\left(T_f - T_\infty\right)$is given by:

$$Nu = -Gr_{x'}^{1/4}\, \theta'(0) \tag{27}$$

The non-dimensional local Sherwood number $Sh = q_m/D\left(C_w - C_\infty\right)$ emerges as:

$$Sh = -Gr_{x'}^{1/4}\, \varphi'(0) \tag{28}$$

Here $\bar{u}_*^{\,2}$ is the characteristic velocity and $Gr_{x'} = g'\beta_{T_0}\left(T_f - T_\infty\right)x'^3/\nu^2$ is the local thermal Grashof number.

3. NUMERICAL SHOOTING QUADRATURE SOLUTION

To obtain the solution of Eq. (20) to Eq. (23) with corresponding boundary conditions (24), we have applied Runge-Kutta fourth order method. The coupled nonlinear ordinary differential equations are converted into simultaneous nonlinear differential equations of first order and further transformed into an initial value problem by applying the

shooting technique. Computational step size is specified as $\Delta\eta = 0.001$ to obtain solutions upto the desired accuracy. The ordinary differential equations (20) to (23) are written as follows:

$$f = y_1,\ f' = y_2,\ \ f'' = y_3,\ h = y_4,\ h' = y_5,\ \theta = y_6,\ \theta' = y_7,\ \phi = y_8,\ \phi' = y_9 \tag{29}$$

$$f''' = (1-N)\left(- y_1 y_3 + y_2^2 - \frac{N}{1-N} y_5 - \cos\alpha\ y_6 - B\cos\alpha\ y_8 \right) \tag{30}$$

$$h'' = \frac{2-2N}{2-N}\left(- y_1 y_5 + y_2 y_4 + \frac{N}{1-N}(2y_4 + y_3) \right) \tag{31}$$

$$\theta'' = -\frac{Pr}{1+R} y_1 y_7 \tag{32}$$

$$\phi'' = -Sc(y_1 y_9 - Kr\ y_8) \tag{33}$$

$$\left.\begin{array}{ll} y_1(0) = f_w, & y_2(0) = 0, \quad y_4(0) = -n\ y_3(0), \\ y_7(0) = -Bi\,(1 - y_6(0)), & y_8(0) = 1, \end{array}\right\} \tag{34}$$

In order to integrate we require with unknown values $y_3(0)$, $y_5(0)$, $y_7(0)$ and $y_9(0)$. Suitable values of $y_3(0)$, $y_5(0)$, $y_7(0)$ and $y_9(0)$ are chosen and integration is performed. Verification of solutions has been performed against Ram Reddy *et al* [48] for the case of vanishing chemical reaction and in the absence of radiative heat flux on a *vertical* plate. The present numerical shooting solutions are compared with those of Ram Reddy *et al* [48] in **Table 1** for shear stress $f''(0)$ at the plate (skin friction), couple stress $h'(0)$, temperature gradient $-\theta'(0)$, (Nusselt number), rate of mass transfer, $-\phi(0)$ (Sherwood number). Very good correlation is achieved.

	$f''(0)$	$h'(0)$	$-\theta'(0)$	$-\phi'(0)$
Shooting Method	0.6779733	-0.338987	0.0773751	0.2290111
Ram Reddy *et al.* [48]	0.6779733	-0.338987	0.0773751	0.2290111

Table 1: Validation of shooting numerical code with published studies [48] for $N = 0.5$, $n = 0$, $\alpha = 0$ (vertical plate), $Pr = 0.71$, $Bi = 0.1$, $B = 1$ and all other parameters negated in general model.

4. GENERAL NUMERICAL VALIDATION WITH ADM

To verify the accuracy of the generalized micropolar model with all parameters invoked, an alternative numerical method is required. We employ the efficient Adomian decomposition method (**ADM) which is** a semi-numerical

technique utilizing special Adomian polynomials to achieve very accurate solutions which may be evaluated using symbolic packages such as Mathematica. An advantage of this method is that it can provide analytical approximation or an approximated solution to a wide class of nonlinear equations without linearization, perturbation closure approximation or discretization methods. ADM has found great popularity in modern engineering sciences and has been implemented in periodic (pulsatile) Newtonian flows [61], Sisko non-Newtonian thin film flows [62], enzyme dynamics [63], bio-magnetic orthopaedic lubrication flows [64]. It has also been successfully used in micropolar hydrodynamics in channels [65], second law thermodynamic analysis of multi-mode heat transfer in micropolar porous media flows [66] and stagnation-point micropolar flows [67]. ADM [35] deploys an infinite series solution for the unknown functions and utilizes recursive relations. For example, for the Eqns. (14) -(17), we assume infinite series solution for the unknown linear velocity, micro-rotation, temperature and concentration functions $f(\eta)$, $h(\eta)$, $\theta(\eta)$, $\phi(\eta)$, defined as follows:

$$f(\eta)=\sum_{n=0}^{\infty} f_n(\eta) \tag{35}$$

$$h(\eta)=\sum_{n=0}^{\infty} h_n(\eta) \tag{36}$$

$$\theta(\eta)=\sum_{n=0}^{\infty} \theta_n(\eta) \tag{37}$$

$$\varphi(\eta)=\sum_{n=0}^{\infty} \phi_n(\eta) \tag{38}$$

The components $f_0, f_1, f_2 ....., h_0, h_1, h_2 ....., \theta_0, \theta_1, \theta_2 .....$ and $\phi_0, \phi_1, \phi_2 .....$are usually determined recursively by an appropriate relation, as elaborated further by Bég *et al.* [68]. The resulting decomposition series converges very quickly and relatively few terms are needed to achieve high accuracy. **Table 2** presents the comparison between shooting and ADM solutions for selected values of certain parameters. Excellent correlation is obtained. Confidence in the shooting solutions for the general micropolar transport model is therefore very high.

Table-2: Skin friction coefficient, couple stress coefficient, Nusselt number and Sherwood number for fixed values of $Pr = 0.71, Bi = 0.1, B = 1$ with both shooting quadrature and ADM.

N	n	α	f_w	R	Sc	Kr	$f''(0)$	$h'(0)$	$-\theta'(0)$	$-\phi'(0)$
0	0	π/2	0.1	0.5	0.22	0	2.6573667 (shooting)	8.4615193	0.0556598	0.111403
"	"	"	"	"	"	"	2.6574001 ADM	8.4616432 ADM	0.0556610 ADM	0.111397 ADM
0.5	0	0	0.1	0.5	0.22	0	0.6779733 (shooting)	-0.338987	0.0773751	0.2290111
"	"	"	"	"	"	"	0.6779804 ADM	-0.338996 ADM	0.0773762 ADM	0.2290126 ADM
0.5	1.5	π/4	0.1	0.5	0.22	0	1.1096598 (shooting)	-1.66449	0.0790626	0.2483065
"	"	"	"	"	"	"	1.1096607 ADM	-1.66463 ADM	0.0790648 ADM	0.2483101 ADM
0.5	0.5	π/4	0.1	0.5	0.22	0.1	0.6634934 (shooting)	-0.331747	0.0771155	0.2668805
"	"	"	"	"	"	"	0.6634951 ADM	-0.331765 ADM	0.0771172 ADM	0.266822 ADM

5. NUMERICAL SHOOTING QUADRATURE RESULTS AND DISCUSSION

A detailed set of solutions for the influence of the key control parameters is presented in **Table 3** and visualized in **Figures 2-14**. In the graphs we illustrate the impact of Eringen micropolar coupling number, angle of inclination, suction/injection parameter, radiation-conduction parameter, Biot number and chemical reaction parameter on the velocity, angular velocity, temperature and concentration functions. In **Table 3** we document the shooting solutions for shear stress $f''(0)$ at the plate(skin friction), couple stress $h'(0)$, temperature gradient $-\theta'(0)$, (Nusselt number), rate of mass transfer, $-\phi(0)$ i.e. (Sherwood number) at the plate for different values of $N, \Lambda, \alpha, f_w, R, Sc,$ and Kr. **Inspection of Table 3** reveals that as suction, radiation and surface condition parameter increase, skin friction and couple stress coefficients both increase in magnitude whereas the reverse trend is observed with an increase in the values of material parameter, Schmidt number, injection and chemical reaction parameter. Also, Nusselt number *i.e. wall heat transfer rate* and Sherwood number *i.e. rate of mass transfer* rare both reduced with an increase in suction and surface condition parameter whereas material parameter and thermal radiation induce the converse effect. Moreover, as Schmidt number and chemical reaction parameter (destructive i.e. *Kr* negative) increase, Sherwood

number increases whereas increasing constructive chemical reaction (positive *Kr*) manifests in a decrease in Sherwood number. Hence heavier species achieves favorable enhancement in the rate of species diffusion (mass transfer) at the wall.

Table-3: Shooting solutions for skin friction coefficient, couple stress coefficient, Nusselt number and Sherwood number for the fixed values of $Pr = 0.71, Bi = 0.1, B = 1$.

N	n	α	f_w	R	Sc	Kr	$f''(0)$	$h'(0)$	$-\theta'(0)$	$-\phi'(0)$
0	0	π/2	0.1	0.5	0.22	0	2.6573667	8.4615193	0.0556598	0.111403
0		π/4					0.8893763	-0.444688	0.0782222	0.2370888
0.5							0.6779733	-0.338987	0.0773751	0.2290111
	1.5						1.1096598	-1.66449	0.0790626	0.2483065
	0.5		0				0.6704779	-0.335239	0.0759218	0.2174584
			-0.1				0.6629606	-0.33148	0.0743411	0.2062957
			0.1	0.3			0.6711521	-0.335576	0.0785741	0.2281409
				0.1			0.6637289	-0.331864	0.0799077	0.2272447
				0.5	0.6		0.6056885	-0.302844	0.075762	0.3560022
					0.78		0.5853579	-0.292679	0.0752676	0.4007132
					0.22	-0.1	0.6944734	-0.347237	0.077656	0.1871738
0.5	0.5	π/4	0.1	0.5	0.22	0.1	0.6634934	-0.331747	0.0771155	0.2668805

Fig. 2 shows the effect of coupling number on velocity distribution with all other pertinent parameters constrained. The coupling number N characterizes the coupling of rotational and linear motion arising from the fluid particles. It is interesting to observe that with an increase in coupling number N linear velocity is reduced i.e. flow deceleration is caused, closer to the plate surface. However, the reverse effect is enforced with further distance from the plate. This variation is probably associated with the space available for gyration of micro-elements. With greater *N* values the micropolar vortex viscosity is increased relative to the dynamic Newtonian viscosity. This impedes rotation nearer the wall but further into the boundary layer it aids gyration of micro-elements. Via coupling with the linear momentum field i.e. the term, $+\left(\frac{N}{1-N}\right)h'$, the linear velocity is therefore *damped* closer to the plate surface whereas it is enhanced further from it. The coupling number clearly modifies the linear velocity field substantially as is anticipated from the significant contribution of the high order shear term, $\left(\frac{1}{1-N}\right)f'''$ in eqn. (20). The findings concur with

numerous other investigations in the literature including Rahman *et al.* [39] and Das [40], in particular the drag enhancement closer to the boundary and drag reduction further from it. Asymptotically smooth convergence of profiles in the free stream is achieved confirming the imposition of an adequately large infinity boundary condition in the shooting numerical code.

Fig. 3illustrates the effect of coupling number on micro-rotation distribution, h (η). Micro-rotation is significantly enhanced with greater N values since the micropolar vortex viscosity is increased relative to the dynamic Newtonian viscosity. The profiles grow from the plate surface markedly and vanish in the asymptotic limit in the free stream. In the Newtonian case (N =0) the micro-rotation equation is negated. With increasing N there is a progressively greater micro-rotation overshoot which is progressively displaced further from the wall. Generally leading to an following this overshoot the negative angular velocities become positive indicating a reversal in micro-rotation of micro-elements. The maximum micro-rotation therefore arises at intermediate distances from the plate surface. This may be associated with the absence of antisymmetric part of the stress. It is certainly intimately associated with enhanced freedom of micro-elements to spin, even with greater concentrations, a characteristic which is stifled near and at the plate surface.

Fig. 4depicts the impact of plate angle of inclination on translational velocity profiles. It is clearly observed that velocity is decreased with greater inclination. The inclination is simulated via the appropriate thermal and species buoyancy forces in the linear momentum equation i.e. $+\theta \cos\alpha, +B\varphi \cos\alpha$. As α increases these thermal and combined species/thermal buoyancy forces decrease. The maximum buoyancy force arises for $\alpha \to 0$ *i.e.* $\cos\alpha \to 1$ which corresponds to the vertical plate scenario. The minimum buoyancy force is associated with $\alpha \to \pi/3$ *i.e.* $\cos\pi/2 \to 0.5$. In the present computations we vary the plate inclination from the vertical case through $\pi/6$, then $\pi/4$ and finally $\pi/6$. The horizontal plate case i.e. $\alpha \to \pi/2$ *is not considered.* The implication is therefore that the convective currents generating buoyancy diminish in influence with greater plate inclination and this decelerates the linear velocity field. Momentum development is inhibited significantly more the majority of the boundary layer regime with the most prominent effect closer to the plate surface. For the range of inclinations studied the buoyancy forces are effectively halved in magnitude.

Fig. 5 presents the effect of inclination on micro-rotation profiles. Closer to the plate surface, initially as α increases there is distinct acceleration in angular velocity (micro-rotation) profiles with decreasing buoyancy forces. The depletion in linear momentum is compensated for by a boost in angular momentum via coupling of the two momenta

equations. These terms are $\left(\frac{1}{1-N}\right) f''', +\left(\frac{N}{1-N}\right) h'$ in eqn. (20) and $+ f\, h', - f'\, h, -\left(\frac{N}{1-N}\right)(2h + f'')$ in eqn. (21). The former are linear terms whereas the latter are strongly non-linear. Both exert a considerable indirect influence from the buoyancy force in the linear momentum field on the angular momentum field. In the *near-wall* zone angular velocity is always negative indicating spin reversal of micro-elements. This is associated both with the surface boundary condition and the constraint on micro-elements which cannot perform gyratory motions with the same freedom near a solid boundary. Similar findings have been reported by Guram and Smith [49] and Ahmadi [50] although they only considered flat plate scenarios. However, with further progress into the boundary layer transverse to the wall, the micro-elements are provided with greater space for spinning and magnitudes are substantially boosted and positive. The prescribed vanishing micro-rotation boundary condition in the free stream is also approached very smoothly again indicating the prescription of a sufficiently large infinity boundary condition in the shooting program. **Fig. 6 and 7** exhibits the effect of plate inclination (α) on both temperature and concentration evolution. Increasing plate inclination decreases both thermal buoyancy force and thermal: species buoyancy force magnitudes. This serves to strongly elevate the temperature (fig. 6). The micropolar fluid is in contact with the hot plate surface. Heat induces a molecular separation and scattering resulting in less dense micropolar fluid. This generates migration of fluid and increasing density in cooler fluid. The boost in natural convection current enhances thermal diffusion which elevates temperatures in the boundary layer as the hotter volume transfers heat towards the cooler volume of fluid. Thermal boundary layer thickness is therefore significantly elevated in the laminar flow. The primary impact is experienced via the thermal buoyancy term, $+\theta \cos\alpha$ which couples the linear momentum field to the temperature field. However, with regard to the species concentration (fig. 7) the coupling is via the composite buoyancy force term i.e. $+B\varphi\cos\alpha$. This connects the linear momentum field (20) to the species field (23). Coupling is further enforced via the convective diffusion term, $+Sc\, f\, \varphi'$ in eqn. (23). In the same way that heat induces molecular separation, changes in concentration buoyancy force modify the species diffusion through the micropolar fluid. As expected species concentration is also significantly boosted with increasing plate inclination owing to the associated depletion in species buoyancy force, which is a characteristic feature of thermo-solutal convection. Concentration boundary layer thickness is therefore also elevated. In both figs 6 and 7, the trends are sustained throughout the boundary layer i.e. there is no cross-over in profiles at any location.

Figs. 8-11 present the response in linear (translational) velocity, angular velocity (micro-rotation component), temperature and concentration profiles to variation in *wall mass flux* i.e. suction/injection parameter (f_w). Here $f_w > 0$ represents suction and $f_w < 0$ denotes injection. Porous surfaces are an inexpensive and established methodology for modifying momentum, thermal and species diffusion characteristics in materials processing [1]. In the case of suction, a markedly lower linear velocity is computed when compared with injection (fig. 8). The extraction of micropolar fluid via the plate pores, destroys momentum in the boundary layer. This causes retardation and a thickening of the hydrodynamic (momentum) boundary layer thickness. The converse effect is generated with injection of micropolar fluid through the wall (blowing) which elevates momentum development and manifests in strong acceleration and a thinner velocity boundary layer thickness. Drag is therefore reduced with injection and increased with suction. The velocity overshoot near the plate is also trans-located steadily towards the plate with greater suction owing to the enhanced adhering of the boundary layer to the plate. Separation and back flow are never observed irrespective of the nature or strength of the lateral mass flux condition (f_w). The solid wall case, f_w=0, evidently is intercalated between the suction and injection profiles. Fig. 9 indicates that the response in micro-rotation to lateral mass flux is dependent in the location in the boundary layer transverse to the wall i.e. η-coordinate. In close proximity to the wall, injection induces a weak acceleration in spin of micro-elements. However, this is reversed further from the wall where injection decelerates the angular velocity. The trend is further reversed again deeper into the boundary layer in the post-overshoot region. Here suction is found to accelerate the micro-rotation. Clearly therefore the behavior of micro-elements is space-dependent and depending on the location the mass flux wall condition exerts a different influence. Figures 10 and 11 demonstrate that both temperature and concentration of the fluid is elevated with wall injection, whereas it is suppressed with wall suction. The associated thermal and solutal (species) boundary layer thicknesses are therefore both increased with greater blowing effect (injection) which is inevitably induced by the enhancement in thermal and species diffusion with momentum development. The different wall temperatures are caused by the thermal convective boundary condition, associated with the Biot number in eqn. (24). Concentration at the wall however is always unity as the convective boundary condition does not influence the species field at the plate.

Fig. 12 illustrates the impact of the radiation effect on temperature profiles. It is observed that an increase in radiation parameter enhances the temperature magnitudes substantially. The radiation-conduction parameter,

$R = 16\bar{\sigma}T_\infty^3 / 3\bar{k}\kappa$ relates the relative input of thermal radiative heat transfer to thermal conduction heat transfer. This is a reasonable approximation for optically thick micropolar flows, as considered here. This approximation however cannot simulate variation in optical thickness which requires a more sophisticated flux model- see Bég *et al.* [69]. *R* arises in the augmented thermal diffusion term, $(1+R)\theta''$ in the heat conservation eqn. (22). Increasing *R* serves to energize the boundary layer and elevates the input of thermal energy which is scaled with a cubic variation in free stream temperature for thermal radiation compared with the linear variation for thermal conduction. The result is that thermal boundary layer thickness is increased and significant enhancement in thermal diffusion is induced. The case *R* = 0 implies total thermal conduction dominance i.e. vanishing radiative flux and clearly achieves a minimum temperature. Evidently the benefit of high temperature processing of materials is confirmed with radiative transfer contribution.

Fig. 13 exhibits the effect of Biot number Bi on the temperature profiles and demonstrates that a high Biot number indicates higher internal thermal resistance of the plate than boundary layer resistance, i.e. ($\theta(0) = 1$ as $Bi \to \infty$). As Biot number increases, temperature of the fluid increases, although as per the imposition of a convective wall boundary condition, the greatest influence is at the plate surface itself. The impact is diminished with distance from the plate. The "thermally thick" scenario (Biot number > 0.1) is addressed only since this is more relevant to polymeric processing.

Fig. 14 shows the modification in species concentration with both Schmidt number (*Sc*) and chemical reaction parameter (*Kr*). It is seen that as Kr increases positively there is a reduction in concentration. However, with a negative reaction parameter the opposite effect is generated. The chemical reaction model employed is based on a first-order irreversible chemical reaction which takes place both in the bulk of the fluid (homogeneous) as well as at the plate. For the constructive i.e. generative ($Kr > 0$) case, the original species is depleted whereas for the destructive chemical reaction (*Kr*<0) the converse effect is induced. Concentration boundary layer thickness is boosted with greater destructive chemical reaction. An increase in Schmidt number significantly reduces species concentration irrespective of the nature of the chemical reaction.

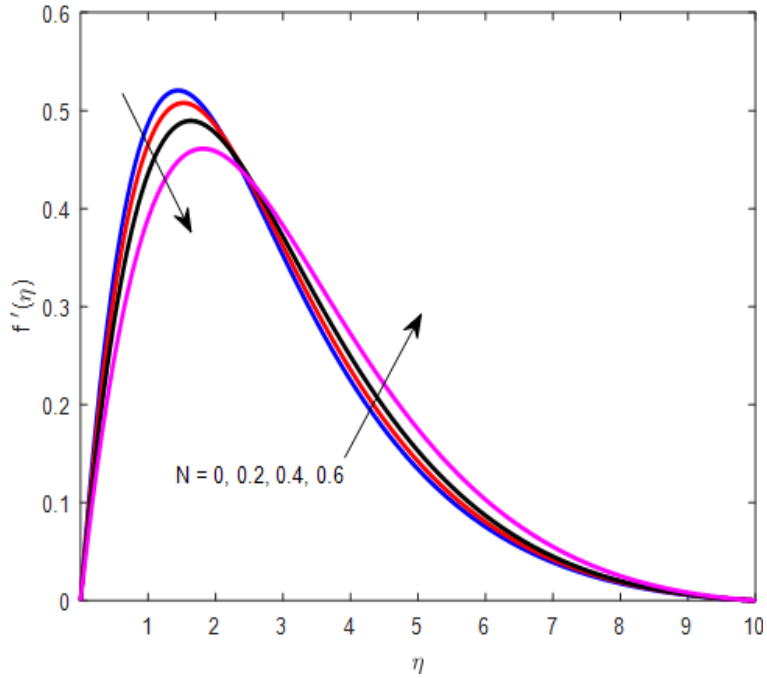

Fig.2 Effect of N on velocity profile for
$n = 0.5, B = 1, \alpha = \pi / 4, R = 0.5, Pr = 0.71, Sc = 0.22, f_w = 0.1, \ Bi = 0.1, Kr = 0$

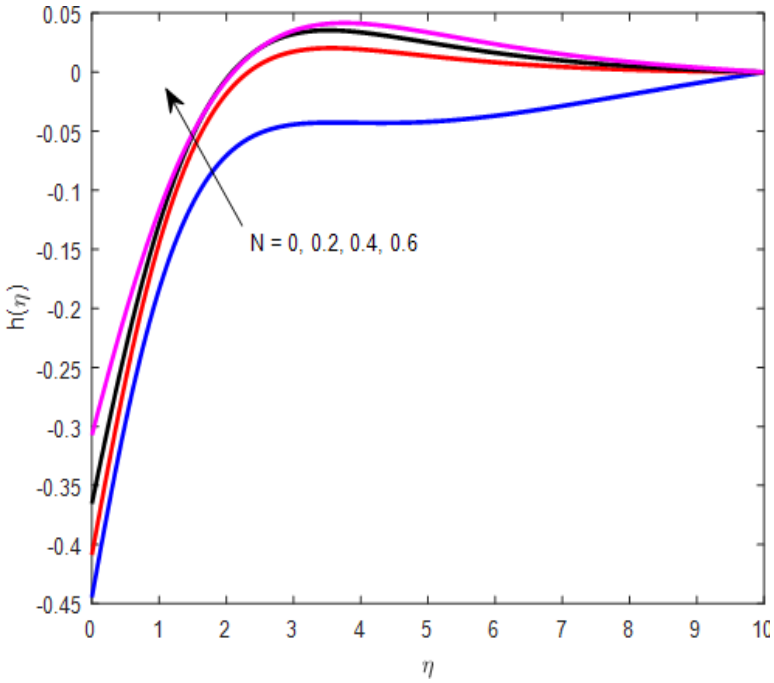

Fig.3 Effect of N on micro-rotation profile for
$n = 0.5, B = 1, \alpha = \pi / 4, R = 0.5, Pr = 0.71, Sc = 0.22, f_w = 0.1, \ Bi = 0.1, Kr = 0$

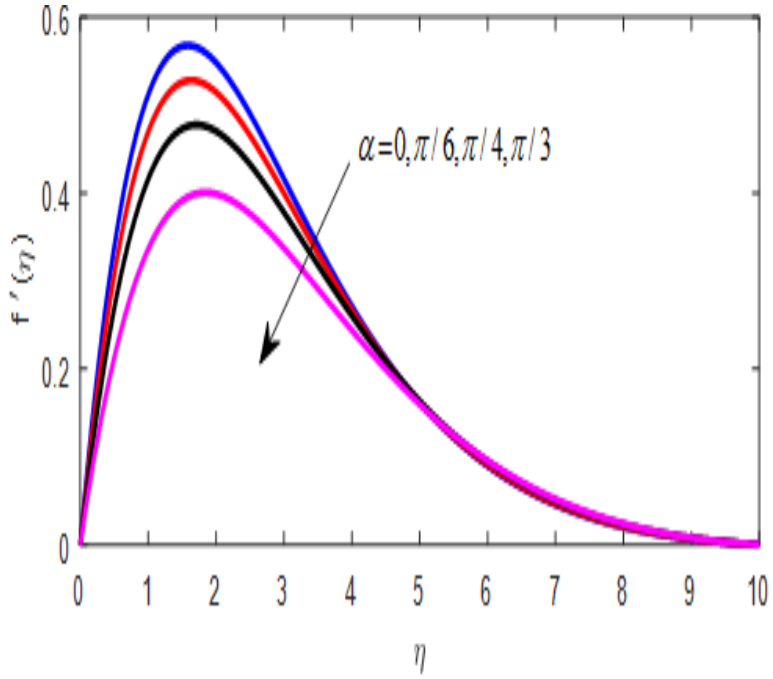

Fig.4 Effect of α on velocity profile for
$n = 0.5, B = 1, R = 0.5, Pr = 0.71, Sc = 0.22, f_w = 0.1,\ \ Bi = 0.1, N = 0.5, Kr = 0$

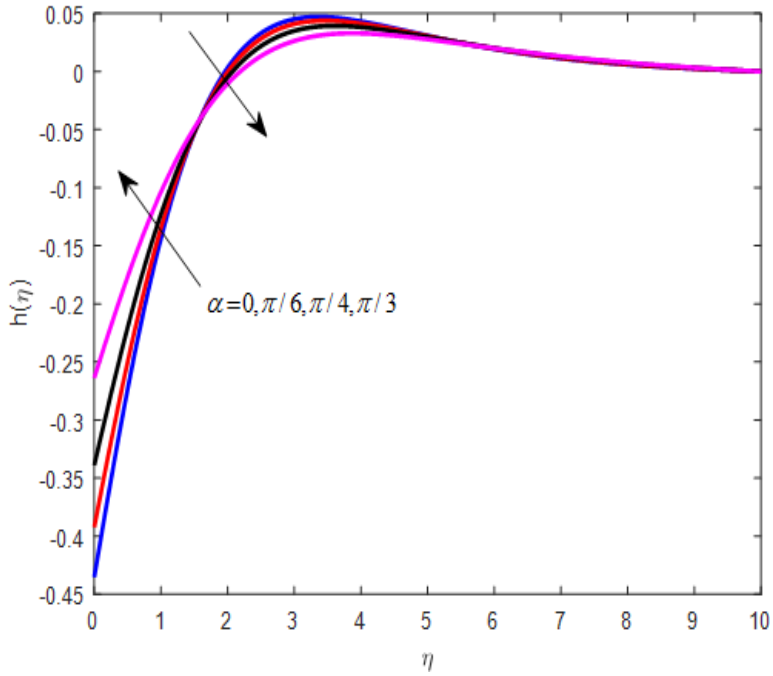

Fig.5 Effect of α on micro-rotation profile for
$n = 0.5, B = 1, R = 0.5, Pr = 0.71, Sc = 0.22, f_w = 0.1,\ \ Bi = 0.1, N = 0.5, Kr = 0$

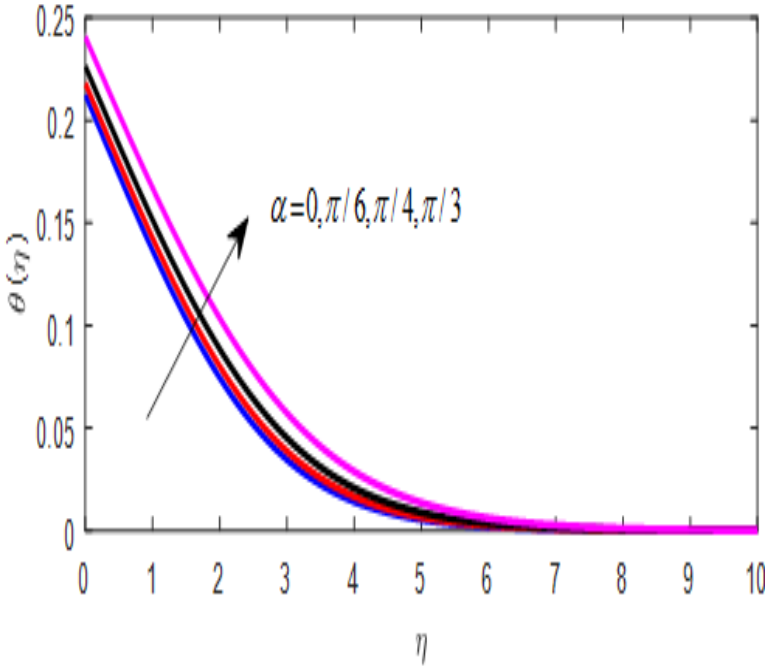

Fig.6 Effect of α on temperature profile for
$n=0.5, B=1, R=0.5, Pr=0.71, Sc=0.22, f_w=0.1,\ Bi=0.1, N=0.5, Kr=0$

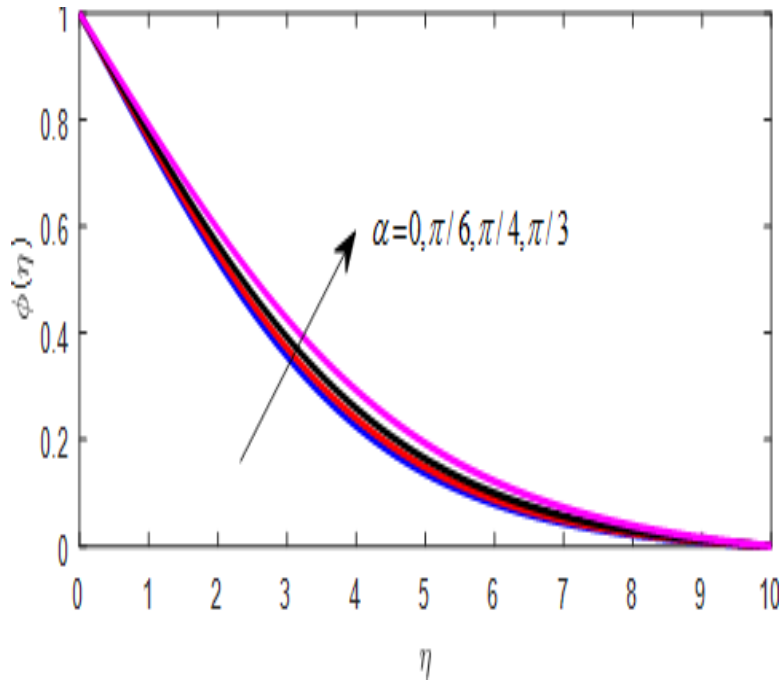

Fig.7 Effect of α on concentration profile for
$n=0.5, B=1, R=0.5, Pr=0.71, Sc=0.22, f_w=0.1,\ Bi=0.1, N=0.5, Kr=0$

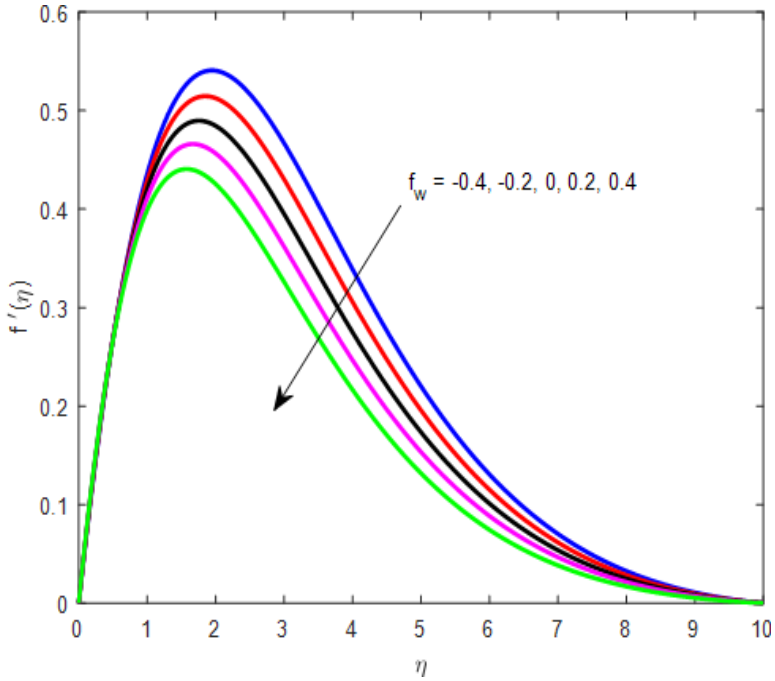

Fig.8 Effect of f_w on velocity profile for
$n = 0.5, B = 1, \alpha = \pi / 4, R = 0.5, Pr = 0.71, Sc = 0.22, Bi = 0.1, N = 0.5, Kr = 0$

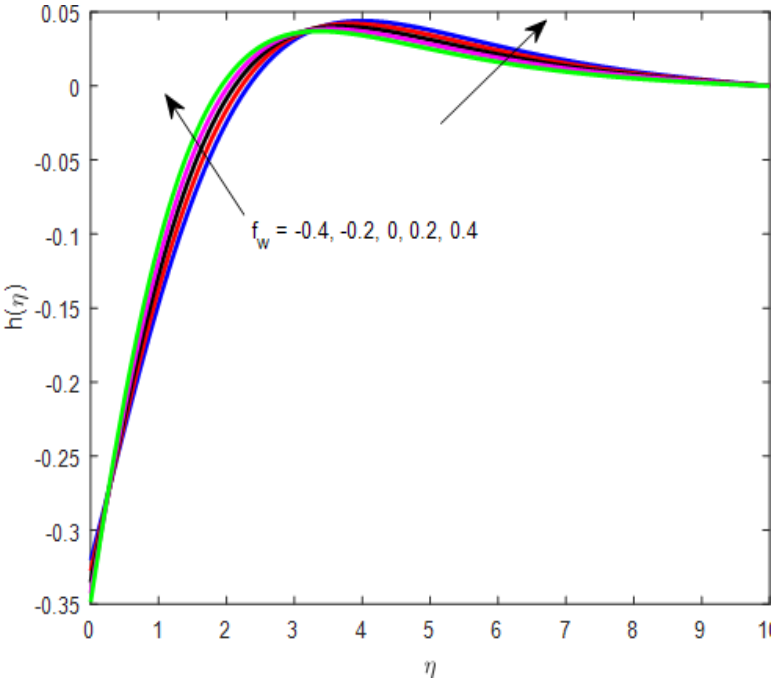

Fig.9 Effect of f_w on micro-rotation profile for
$n = 0.5, B = 1, \alpha = \pi / 4, R = 0.5, Pr = 0.71, Sc = 0.22, Bi = 0.1, N = 0.5, Kr = 0$

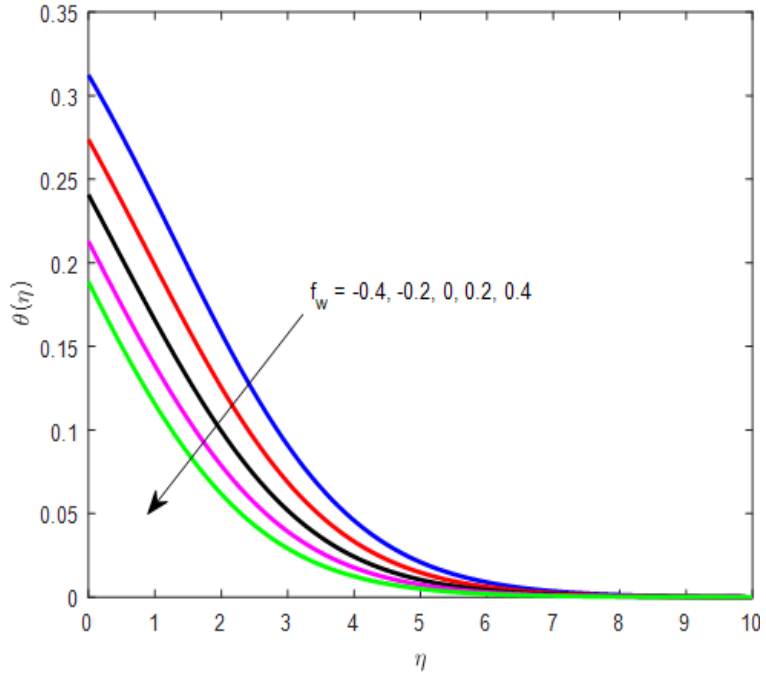

Fig.10 Effect of f_w on temperature profile for
$n = 0.5, B = 1, \alpha = \pi / 4, R = 0.5, Pr = 0.71, Sc = 0.22, Bi = 0.1, N = 0.5, Kr = 0$

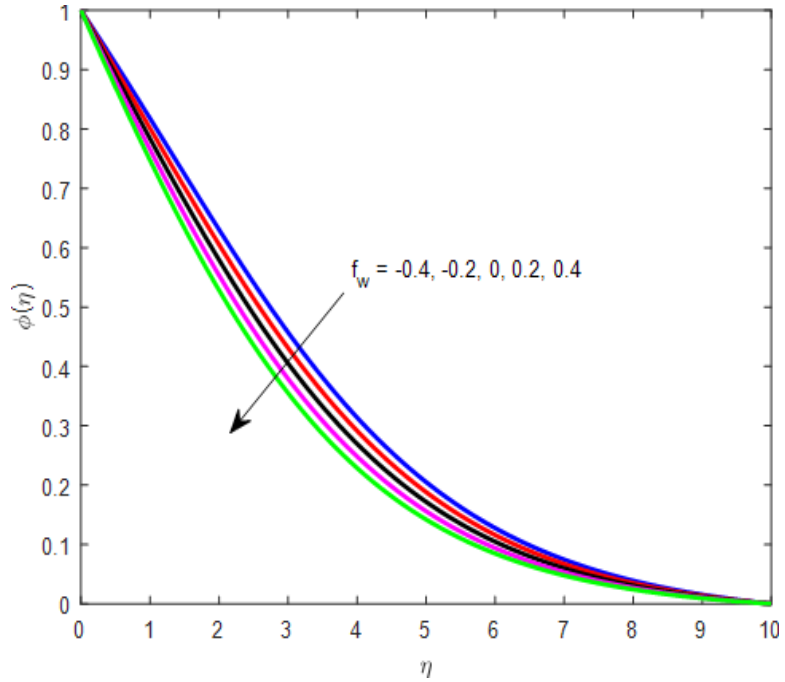

Fig.11 Effect of f_w on concentration profile for
$n = 0.5, B = 1, \alpha = \pi / 4, R = 0.5, Pr = 0.71, Sc = 0.22, Bi = 0.1, N = 0.5, Kr = 0$

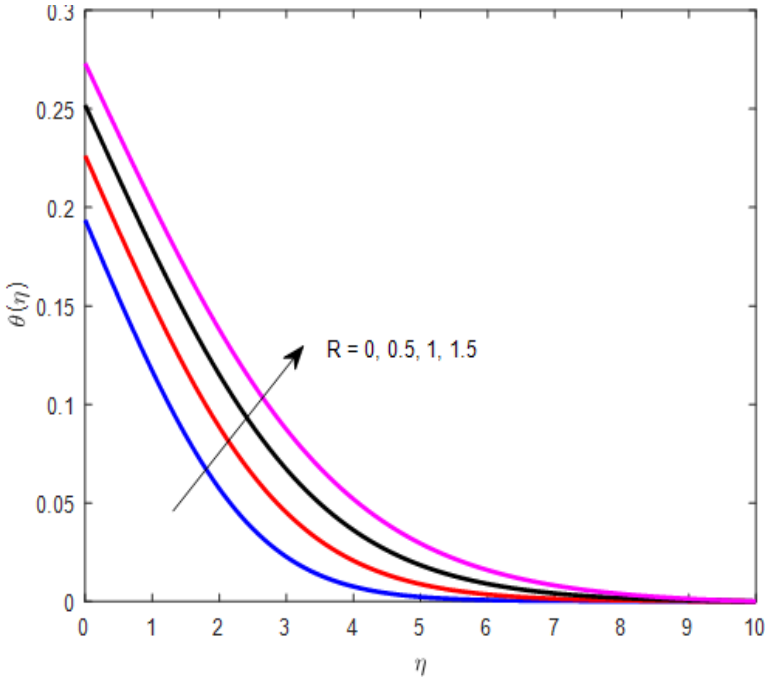

Fig.12 Effect of R on temperature profile for
$n = 0.5, B = 1, \alpha = \pi / 4, Pr = 0.71, Sc = 0.22, f_W = 0.1, Bi = 0.1, N = 0.5, Kr = 0$

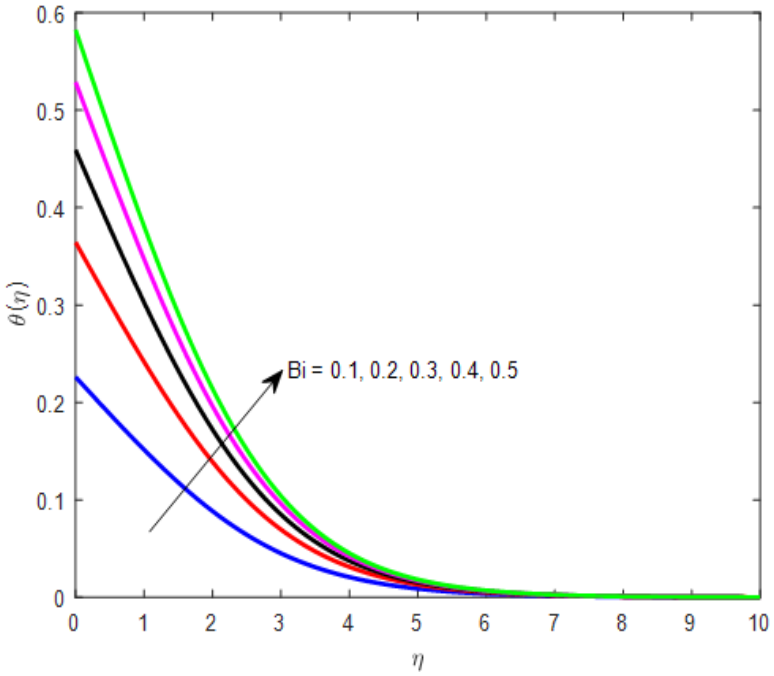

Fig.13 Effect of Bi on temperature profile for
$n = 0.5, B = 1, \alpha = \pi / 4, Pr = 0.71, R = 0.5, Sc = 0.22, f_W = 0.1, N = 0.5, Kr = 0$

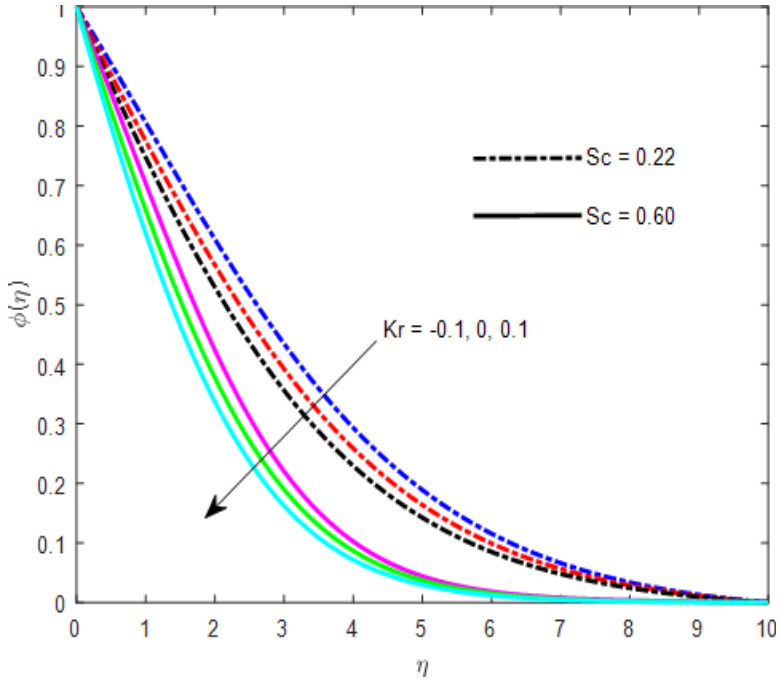

Fig.14 Effect of Sc and Kr on concentration profile for $n = 0.5, B = 1, \alpha = \pi / 4, Pr = 0.71, R = 0.5, f_w = 0.1, N = 0.5, Bi = 0.1$

6. CONCLUDING REMARKS

A steady-state mathematical model has been presented for laminar, incompressible, thermo-solutal natural convection flow of micropolar transport from a tilted porous plate with convective boundary conditions. Both chemical reaction and radiative heat transfer have also been considered. Via Lie scaling group algebraic transformations, a self-similar boundary value problem has been derived in ordinary differential form. This 9th order, multi-degree system is solved subject to physically realistic boundary conditions with 4th order numerical quadrature and a shooting technique. Verification of solutions has been conducted against published literature (for the non-reactive, non-radiative vertical plate case) and also with a modified Adomian decomposition method (ADM) (for the generalized multi-physical model with all parameters present). Selected computations have been visualized graphically. The study has shown that:

- Increasing plate inclination (α) decelerates the linear velocity, accelerates micro-rotation near the plate and also enhances the temperature and concentration magnitudes.
- Increasing suction effect decreases the linear velocity and skin friction, wall couple stress (micro-rotation gradient), Nusselt number and Sherwood number.

- Increasing Eringen micropolar coupling number decreases translation velocity near the plate whereas it accelerates it further form the plate. Furthermore, micro-rotation is boosted strongly with greater coupling number.
- Increasing radiative effect and Biot number (convective surface effect) both elevate the temperature magnitudes.
- Increasing positive chemical reaction parameter depresses concentration magnitudes.
- Increasing Schmidt number reduces species concentration boundary layer thickness.

FUTURE SCOPE:

The present model has considered Fourier conduction and Fickian diffusion approaches. Future studies will explore non-Fourier (Cattaneo) models which incorporate thermal relaxation and also non-Fickian models, both of which may provide more elegant insight into polymer processing systems.

REFERENCES

[1] Kou S (1996) Transport Phenomena and Materials Processing, Wiley, New York, USA.

[2] Jarny S, Roussel N, Le Roy R, Coussot P (2008) Thixotropic behaviour of fresh cement pastes from inclined plane flow measurements. Applied Rheology, 18:14251-1 14251-8.

[3] Suzuki A, Tanka T (1971) Measurement of flow properties of powers along an inclined plane. Ind Eng Chem Fundam, 10:84-91.

[4] Astarita G, Mariucxi G, Palumbo G (1964) Non-Newtonian gravity flow on inclined surfaces. Ind Eng Chem Fundam, 3:333-339.

[5] Hunt B (1994) Newtonian fluid mechanics treatment of debris flows and avalanches. ASCE Hydraul Eng, 120: 1350-1363.

[6] Huang X, Garcia MH (1998) A Herschel–Bulkley model for mud flow down a slope. J Fluid Mech, 374:305-333.

[7] Tari I, Mehrtash M (2013) Natural convection heat transfer from inclined plate-fin heat sinks. Int J Heat and Mass Transfer, 56:574-593.

[8] Rana P, Bhargava R, Bég O. Anwar (2013) Finite element modeling of conjugate mixed convection flow of Al_2O_3–water nanofluid from an inclined slender hollow cylinder. Phys Scr, 87:055005.

[9] Lamarche L (2011) Analytical g-function for inclined boreholes in ground-source heat pump system. Geothermic, 40:241–249.

[10] Kashiwagi T, Newman DL (1976) Flame spread over an inclined thin fuel surface. Combustion and Flame, 26: 163-177.

[11] Mai CC, Lin J (2002) Flow structures around an inclined substrate subjected to a supersonic impinging jet in laser cutting. Optics & Laser Technology, 34:479-486.

[12] Aybar HS (2006) Mathematical modeling of an inclined solar water distillation system. Desalination, 190:63-70.

[13] Fard MH, Hooman K, Chua HT (2010) Numerical simulation of a supercritical CO_2 geothermosiphon. Int Commun Heat and Mass Transfer, 37: 447-51.

[14] Shaukatullah H, Gebhart B (1978) An experimental investigation of natural convection flow on an inclined surface. Int J Heat Mass Transfer, 21:1481-1490.

[15] Hasan MM, Eichhorn R (1979) Local non-similarity solution of free convection flow and heat transfer on an inclined isothermal plate. ASME J Heat Transfer, 101:642-647.

[16] Cianfrini C, Corcione M, D'Orazio A, Habib E (2008) Natural convection heat transfer from vertical and inclined plates facing upwards and downwards. HEFAT2008 6th International Conference on Heat Transfer, Fluid Mechanics and Thermodynamics, Pretoria, South Africa.

[17] Vasu B, Gorla RSR, Murthy PVSN, Prasad VR (2016) Free convection flow of non-Newtonian power-law liquid film with nanoparticles along an inclined plate. 20thAustralasian Fluid Mechanics Conference, Perth, Australia.

[18] Miladinova S, Lebon G, Toshev E (2004) Thin-film flow of a power-law liquid falling down an inclined plate. J Non-Newtonian Fluid Mech, 122:69-78.

[19] Rahman MM, Salahuddin KM (2010) Study of hydromagnetic heat and mass transfer flow over an inclined heated surface with variable viscosity and electric conductivity. Commun Nonlinear Sci Numer Simulat, 15: 2073-2085.

[20] Usha R, Uma B (2004) Long waves on a viscoelastic film flow down a wavy incline. Int J Non-Linear Mech, 39: 1589-1602.

[21] Hayat T, Ellahi R, Mahomed FM (2008) Exact solutions for thin film flow of a third grade fluid down an inclined plane. Chaos Solitons Fractals, 38:1336–1341.

[22] Cochard S, Ancey C (2009) Experimental investigation of the spreading of viscoplastic fluids on inclined planes. J Non-Newtonian Fluid Mech. 158:73-84.

[23] Bognár G, Gombkötő I, Hriczó K (2011) Non-Newtonian fluid flow down an inclined plane. Recent Advances in Fluid Mechanics and Heat & Mass Transfer, 129-134.

[24] Chaturani P, Upadhya VS (1977) Gravity flow of a fluid with couple stress along an inclined plane with application to blood flow. Biorheology, 14:237-246.

[25] Eringen AC (1966) The theory of micropolar fluids. J Math Mech, 16:1-18.

[26] Ariman T, Cakmak AS (1968) Some basic viscous flows in micropolar fluids. Rheologica Acta, 7 (3):236-242.

[27] Ganghoffer JF, Brillard A, Brost RD (1998) Description of the mechanical behaviour of micropolar adhesives. Math Comput Modelling. 27(7):2349-2358.

[28] Bhargava R, Sharma S, Bég O. Anwar, Zueco J (2010) Finite element study of nonlinear two-dimensional deoxygenated biomagnetic micropolar flow. Commun Nonlinear Sci Numr Simult. 15:1210-1233.

[29] Črnjarić-Žic N (2016) Upwind numerical approximations of a compressible 1d micropolar fluid flow. J Comput Appl Math, 303: 81-92.

[30] Bég O. Anwar, Rashidi MM, Bég TA, Asadi M (2012) Homotopy analysis of transient magneto-bio-fluid dynamics of micropolar squeeze film: a model for magneto-bio-rheological lubrication. J Mechanics in Medicine and Biology, 12(3): 1250051-1 to 1250051-21.

[31] Shelukhin VV, Neverov VV (2016) Thermodynamics of micropolar Bingham fluids. J Non-Newtonian Fluid Mech, 238:16-23.

[32] Prasad VR, Gaffar SA, Bég O. Anwar (2015) Heat and mass transfer of a nanofluid from a horizontal cylinder to a micropolar fluid. AIAA J Thermophysics Heat Transfer, 29(1):127-139.

[33] Annapurna N, Ramanaiah G (1976) Effect of couple stresses on the unsteady drainage of a micro-polar fluid on a flat surface. Japanese J Appl Phys, 15(12):2441-2244.

[34] Zueco J, Bég O. Anwar, Takhar HS (2009) Network numerical analysis of magneto-micropolar convection through a vertical circular non-Darcian porous medium conduit. Comput Mat Sci. 46(4):1028-1037.

[35] Ravi Kiran G, Radhakrishnamacharya G, Bég O. Anwar (2017) Peristaltic flow and hydrodynamic dispersion of a reactive micropolar fluid: simulation of chemical effects in the digestive process. J Mechanics in Medicine and Biology. doi: 10.1142/S0219519417500130.

[36] Bég O. Anwar, Motsa SS, Kadir A, Bég TA, Islam MN (2016) Spectral quasilinear numerical simulation of micropolar convective wall plumes in high permeability porous media. J Engineering Thermophysics, 25 (4):1–24.

[37] Eringen AC (2001) Micro-continuum Field Theories-II Fluent Media, Springer, New York, USA.

[38] Wilson AJ (1968) The flow of a micropolar liquid layer down an inclined plane. Proceedings of the Cambridge Philosophical Society, 64:513-520.

[39] Rahman MM, Aziz A, Al-Lawatia MA (2010) Heat transfer in micropolar fluid along an inclined permeable plate with variable fluid properties. Int J Thermal Sci, 49:993-1002.

[40] Das K (2012) Slip effects on heat and mass transfer in MHD micropolar fluid flow over an inclined plate with thermal radiation and chemical reaction. Int J Num Meth Fluids, 70: 96-113.

[41] Srinivasacharya D, Hima Bindu K (2016) Entropy generation in a micropolar fluid flow through an inclined channel. Alexandria Eng J, 55:973-982.

[42] Bég O. Anwar, Zueco J, Chang TB (2010) Numerical analysis of hydromagnetic gravity-driven thin film micropolar flow along an inclined plane. Chem Eng Commun, 198(3):312- 331.

[43] Kim IH, Cho HC, Bae YC, Chung KS (2003) Heat and radiation effect on the degradation behaviors of polymeric liquids. European Polymer Journal, 39:1431-1435.

[44] Cortell R (2014) MHD (magneto-hydrodynamic) flow and radiative nonlinear heat transfer of a viscoelastic fluid over a stretching sheet with heat generation/absorption. Energy, 74:896-905.

[45] Fedorov AG, Lee KH, Viskanta R (1998) Inverse Optimal Design of the Radiant Heating in Materials Processing and Manufacturing. J Materials Engineering and Performance, 1(6):719-726.

[46] Viskanta R (1964) Heat transfer in a radiating fluid with slug flow in a parallel-plate channel. Applied Scientific Research, 13(1):291–311.

[47] Adomian G (1994) Solving Frontier Problem in Physics: The Decomposition Method. Kluwer Academic publishers, Boston, USA.

[48] Ram Reddy Ch, Pradeepa T, Srinivasacharya D (2015) Similarity solution for free convection flow of a micropolar fluid under convective boundary condition via Lie scaling group transformations. Advances in High Energy Physics, Article ID:650813 (16 pages). doi:10.1155/2015650813.

[49] Guram GS, Smith AC (1980) Stagnation point flows of micropolar fluids with strong and weak interactions. Computers and Mathematics with Applications, 6:231-233.

[50] Ahmadi G (1976) Self-similar solution of incompressible micropolar boundary layer flow over a semi-infinite plate. Int J Eng Sci, 14:639-646.

[51] Peddieson J (1972) An application of the micropolar fluid model to the calculation of turbulent shear flow. Int J Eng Sci, 10:23-32.

[52] Stokes VK (1984) Theories of Fluids with Microstructure. Springer, New York, USA.

[53] Bég O. Anwar, Ferdows M, Bég TA, Ahmed T, Wahiduzzaman M, Alam MM (2016) Radiative optically-dense magnetized transient reactive transport phenomena with cross diffusion and dissipation effects: numerical simulations. J Taiwan Inst Chemical Eng, 66:12–26.

[54] Olver PJ (1986) Application of Lie Groups to Differential Equations. Springer, Berlin.

[55] Bluman GM, Kumei S (1989) Symmetries and Differential Equations. Springer-Verlag, Newyork, USA.

[56] Cantwell BJ (2003) Introduction to Symmetry Analysis. Cambridge University Press, UK.

[57] Reddy GV, Chamkha AJ (2015) Lie Group analysis of chemical reaction effects on MHD free convection dissipative fluid flow past an inclined porous surface. Int J Numerical Methods for Heat and Fluid Flow, 25(3): 1557-1573.

[58] Si X, Yuan L, Zheng L, Shen Y, Cao L (2016) Lie group method for modified model of MHD flow and heat transfer of a non-Newtonian fluid with prescribed heat flux over a moving porous plate. J Molecular Liquids, 220:768-777.

[59] Latiff NAA, Uddin MJ, Bég O. Anwar, Ismail AI (2015) Unsteady forced bio convection slip flow of a micropolar nanofluid from a stretching/ shrinking sheet. Proc IMECHE- Part N: J Nanoengineering and Nanosystems. doi: 10.1177/1740349915613817.

[60] Uddin MJ, Bég O. Anwar, Amran N, Ismail AIM (2015) Lie group analysis and numerical solutions for magneto-convective slip flow of a nanofluid over a moving plate with a Newtonian heating boundary condition. Canadian J Physics, 93:1–10

[61] Liu CM (2016) Application of the Adomian Decomposition Method to oscillating viscous flows. Appl Comput Math, 5:121-132.

[62] Siddiqui AM, Ashraf H, Haroon T, Walait A (2013) Analytic solution for the drainage of Sisko fluid film down a vertical belt. Applications & Applied Mathematics, 8:465-470.

[63] Sonnad JR, Goudar CT (2004) Solution of the Haldane equation for substrate inhibition enzyme kinetics using the decomposition method. Math Comp Modell. 40:573-82.

[64] Bég OA, Tripathi D, Sochiand T, Gupta PK (2015) Adomian decomposition method (ADM) simulation of magneto-bio-tribological squeeze film with magnetic induction effects. J Mechanics Medicine Biology, 15: 1550072.1-1550072.23.

[65] Aski FS, Nasirkhani SJ, Mohammadian E, Asgari A (2014) Application of Adomian decomposition method for micropolar flow in a porous channel. Propulsion and Power Research, 3:15-21.

[66] Srinivas J, Adesanya SO, Falade JA, Nagaraju G (2017) Entropy generation analysis for a radiative micropolar fluid flow through a vertical channel saturated with non-Darcian porous medium. Int J Appl Comput Math. doi:10.1007/s40819-017-0322-8.

[67] Adanhounmè V, De Paule Codo F, Adomou A (2012) Solving the Navier Stokes flow equations of micro-polar fluids by Adomian decomposition method. Bull Math Sci Applic, 2:30-37.

[68] Bég O. Anwar, Mabood F, Islam MN (2015) Homotopy simulation of nonlinear unsteady rotating nanofluid flow from a spinning body. Int J Eng Math, Article ID: 272079 (15 pages) doi:10.1155/2015/272079.

[69] Bég O. Anwar, Ali N, Zaman A, Bég TAE, Ayesha S (2016) Computational modelling of heat transfer in annular porous medium solar energy absorber with a P1-radiative differential approximation. J Taiwan Inst Chemical Eng. doi: 10.1016/j.jtice.2016.06.034.